Imaging or Fiber Probe-Based Approach? Assessing Different Methods to Detect Near Infrared Autofluorescence for Intraoperative Parathyroid Identification

Giju Thomas, PhD, Malcolm H Squires, MD, Tyler Metcalf, BS, Anita Mahadevan-Jansen, PhD, John E Phay, MD, FACS

BACKGROUND: Near infrared autofluorescence (NIRAF) can guide intraoperative parathyroid gland (PG) identification. NIRAF detection devices typically rely on imaging and fiber probe-based approaches. Imaging modalities provide NIRAF pictures on adjacent display monitors, and fiber probe-based systems measure tissue NIRAF and provide real-time quantitative information to objectively aid PG identification. Both device types recently gained FDA approval for PG identification but have never been compared directly.

STUDY DESIGN: Patients undergoing thyroidectomy and/or parathyroidectomy were recruited prospectively. Target tissues were intraoperatively visualized with PDE-Neo II (imaging-based) and concurrently assessed with PTeye (fiber probe-based). For PDE-Neo II, NIRAF images were collected from in situ or excised tissues, alongside the surgeon's interpretation of visualized tissues, and retrospectively analyzed in a blinded fashion. The PTeye was concomitantly used to record NIRAF intensities and ratios from the same tissues in real time.

RESULTS: Twenty patients were enrolled for concurrent evaluation with both systems, which included 33 PGs and 19 nonparathyroid sites. NIRAF imaging demonstrated 90.9% sensitivity, 73.7% specificity, and 84.6% accuracy for PG identification when interpreted in real time by the surgeon compared with 81.8% sensitivity, 73.7% specificity, and 78.8% accuracy where images were quantitatively analyzed post hoc by an independent observer. In parallel, NIRAF detection with PTeye yielded 97.0% sensitivity, 84.2% specificity, and 92.3% accuracy in real time for the same specimens.

CONCLUSIONS: Both NIRAF-based systems were beneficial for identifying PGs intraoperatively. Although NIRAF imaging provides valuable spatial information to localize PGs, NIRAF detection with fiber probe provides real-time quantitative information to identify PGs in presence of ambient room lights. (J Am Coll Surg 2019;229:596–608. © 2019 by the American College of Surgeons. Published by Elsevier Inc. All rights reserved.)

Inadvertent damage to or excision of a healthy parathyroid gland (PG) after a total thyroidectomy could result in transient hypocalcemia (<6 months) in 5% to 35% of patients, or permanent hypocalcemia (>6 months) in up to 7% of the patients.[1,2] On the other hand, failed parathyroidectomies can occur in 5% to 10% of patients due to the inability to identify or localize the diseased PG.[3,4] As a result, persistent hyperparathyroidism can

Disclosure Information: Vanderbilt University and Drs Mahadevan-Jansen and Phay have a patent on the near infrared autofluorescence detection technique that has been licensed to AiBiomed Instruments, which encompasses use of the PTeye.

Support: Drs Thomas and Mahadevan-Jansen were supported by funding from the NIH (R01CA212147).

Received July 30, 2019; Revised September 10, 2019; Accepted September 11, 2019.

From the Vanderbilt Biophotonics Center (Thomas, Mahadevan-Jansen), Department of Biomedical Engineering (Thomas, Mahadevan-Jansen), Vanderbilt University, Nashville, TN, and Division of Surgical Oncology, Ohio State University Comprehensive Cancer Center and Ohio State University Wexner Medical Center, Columbus, OH (Squires, Metcalf, Phay).

Correspondence address: John E Phay, MD, FACS, Division of Surgical Oncology, Ohio State University Comprehensive Cancer Center and Ohio State University Wexner Medical Center, 410 W 10th Ave, Columbus, OH 43210. email: john.phay@osumc.edu

https://doi.org/10.1016/j.jamcollsurg.2019.09.003
ISSN 1072-7515/19

Abbreviations and Acronyms

IQR = interquartile range
NIR = near infrared
NIRAF = near infrared autofluorescence
NBR = near infrared autofluorescence-to-background ratio
OR = operating room
PG = parathyroid gland
^{99m}Tc = technetium 99m

occur in these patients, leading to unwarranted repeat operations that can be associated with increased morbidity and costs.[5,6] Ultrasound imaging, ^{99m}technetium (^{99m}Tc)-sestamibi scintigraphy, and CT have demonstrated variable efficacy for preoperative localization of diseased PGs.[7,8] However, these modalities are unable to localize healthy PGs and might not always correlate well with the surgical field of view as observed intraoperatively. Consequently, most surgeons rely on visual identification of healthy or diseased PGs, whereby the accuracy of PG identification is eventually determined by surgical skill and experience.[9-11] When in doubt, a surgeon routinely confirms the identity of PG tissue by sending the specimen for frozen-section analysis that typically requires a wait time of 20 to 30 minutes per sample[12] and has the risk of possible injury to a healthy PG.

The unique discovery of near infrared autofluorescence (NIRAF) in PG tissues demonstrated that optical modalities that detect NIRAF can be exploited for noninvasive and label-free identification of both healthy and diseased PGs with accuracy as high as 97%.[13-16] As demonstrated by the Vanderbilt group, it was observed that PGs emit a stronger NIRAF signal than the adjacent thyroid and other soft tissues in the neck. Since then, several research groups have explored the feasibility of localizing PGs using NIRAF detection with reasonable success.[17-25] Based on the previously mentioned studies that had been applied for PG localization, optical modalities capable of NIRAF detection can be broadly categorized as imaging systems and fiber probe systems. Imaging systems, which are noncontact optical modalities, tend to be either commercially available near infrared (NIR) cameras[19,21] or modified prototypes of existing imaging systems.[15,17,22,25] These imaging systems typically illuminate tissues with NIR light at a specific wavelength and collect the resultant fluorescence emitted from tissues with a handheld camera. A fluorescent image is displayed on an adjacent display monitor and tissues with elevated NIRAF are seen as gray or pseudo-colored images for intraoperative visualization by the surgeon (Fig. 1). In contrast, fiber probe systems involve placing a sterile handheld fiber optic probe in contact with the tissue to capture tissue NIRAF as quantitative data. Although this approach was highly sensitive in PG identification, as evidenced from earlier studies, the data that are obtained in a 'spectral' format cannot be easily interpreted by surgeons.[13,14,16] By improving on the original laboratory-built system, a newer iteration called PTeye (AiBiomed Inc) was recently developed that provides the surgeon with real-time auditory feedback on parathyroid identification, along with a visual bar graph on the device display console (Fig. 2). Compared with the laboratory-built system, PTeye has also demonstrated a high accuracy for PG identification with a relatively simpler user interface and the ability to function even in the presence of ambient operating room (OR) lights, which tends to be a deterrent for most imaging systems.[26,27]

Since modalities that rely on NIRAF detection for label-free PG identification having been successfully validated in several studies,[20,26,28,29] FDA approval for this application was recently granted to Fluobeam, an imaging system, and PTeye, a fiber probe-based system, in 2018.[30,31] However, no study has directly compared the performances of these 2 approaches—imaging vs fiber probe—or assessed the value in PG identification by each modality for the surgeon. The current prospective study was designed to compare the performance between an imaging and fiber probe-based approach in NIRAF detection by using the PDE-Neo II imaging system and the PTeye concurrently for the first time in a preliminary cohort of 20 patients. This study can help determine whether both systems are detecting similar NIRAF phenomena in PG tissues and potentially provide valuable insight into the benefits added by either modality in PG identification/localization inside the OR.

METHODS

Patient recruitment

Eligible patients who underwent thyroidectomy and/or parathyroidectomy between December 2018 and January 2019 at the Ohio State University Comprehensive Cancer Center were prospectively enrolled. This study was conducted in agreement with the Declaration of Helsinki and its amendments, and was approved by the IRB at Ohio State University (IRB# 201640045). Written informed consent was obtained from all enrolled patients before operation. Acquired patient data were stored in compliance with the HIPAA (Health Insurance Portability and Accountability Act) privacy rule. Patients with a diagnosis of renal-induced secondary hyperparathyroidism

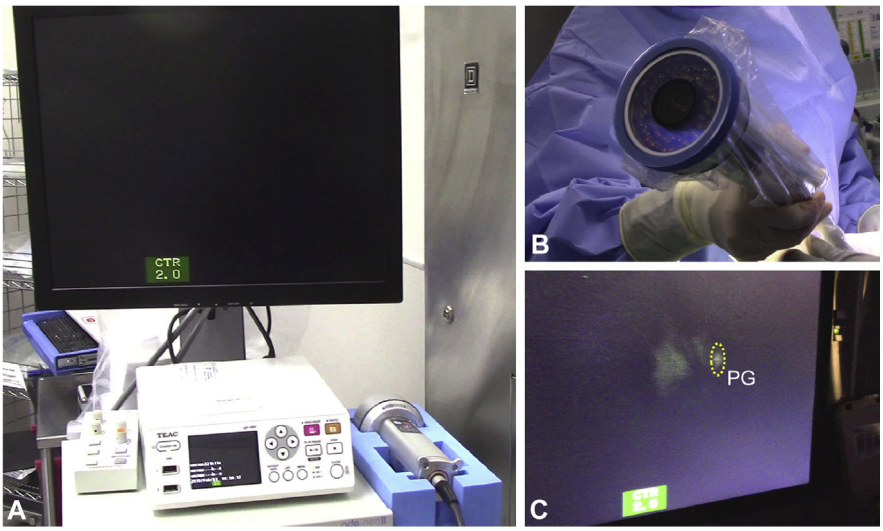

Figure 1. (A) A clinical imaging system (PDE-Neo II) tested for intraoperative parathyroid gland (PG) identification, based on near infrared autofluorescence (NIRAF) detection. (B) The handheld camera of the system is sterile wrapped with a transparent drape before NIRAF imaging. (C) Tissue NIRAF visualized on the remote display monitor of the system in pseudo-colored green. PG tissue (within yellow dashed circle) is observed to have a stronger NIRAF compared with adjacent soft tissue.

were excluded from the study, as earlier studies had demonstrated irregularities in NIRAF observed among these patients.[16,26]

Routine preoperative, intraoperative, and postoperative patient assessment

Patients who underwent parathyroidectomy were preoperatively assessed with ultrasound and/or ^{99m}Tc-sestamibi nuclear imaging to aid in localizing diseased PGs, including parathyroid adenomas. Preoperative serum calcium levels, as well as preoperative, intraoperative, and immediate postoperative parathyroid hormone levels were routinely measured for parathyroidectomy patients, and serum calcium levels were monitored preoperatively and postoperatively for thyroidectomy patients. Excised specimens were subject to standard histopathologic analysis, including tissue type and disease, gross dimensions of the specimen, presence of parathyroid tissue in the specimen, normocellularity/hypercellularity, and weight of excised parathyroid tissue.

Instrumentation of modalities relying on NIRAF detection

PDE-Neo II (Hamamatsu, Mitaka USA, Inc) used for imaging in this study comprises a handheld camera, a console for adjusting image acquisition parameters, and a display monitor mounted on a portable stand (Fig. 1). The camera of PDE-Neo II emits NIR light at a wavelength of 760 nm using a light-emitting diode, with the device being categorized as a 1-M light-emitting diode product. White-light (true color) and NIRAF (gray/pseudo-colored green) images are relayed to the display monitor for visualization by the surgeon, as ambient OR lights are switched off during the procedure. In comparison, the fiber probe-based device, PTeye (Fig. 2), comprises a console that consists of a 785 nm laser diode and a detector, a detachable fiber (optic) probe, and a foot pedal to activate NIRAF measurements. PTeye is also capable of detecting NIRAF without interference from ambient OR lights as well, due to the internal circuitry designed for the system. Tissue NIRAF recorded with PTeye is conveyed to a display panel of the console as well as to a loudspeaker for auditory feedback. The display panel informs the surgeon on the detection level (absolute tissue NIRAF intensity) and the detection ratio (tissue NIRAF normalized to the baseline NIRAF intensity), which is translated into a percentage likelihood that the tissue is parathyroid. The auditory feedback initiates when the detection ratio exceeds 1.2—the threshold value set for PG identification.[26]

Comparative study with concurrent NIRAF detection with PDE-Neo II and PTeye

During the operation, tissue was identified as possible PG tissue by the surgeon and left in situ. Before NIRAF image acquisition, the handheld camera of PDE-Neo II was wrapped with a sterile transparent drape and positioned approximately 5 cm above the surgical field. After the

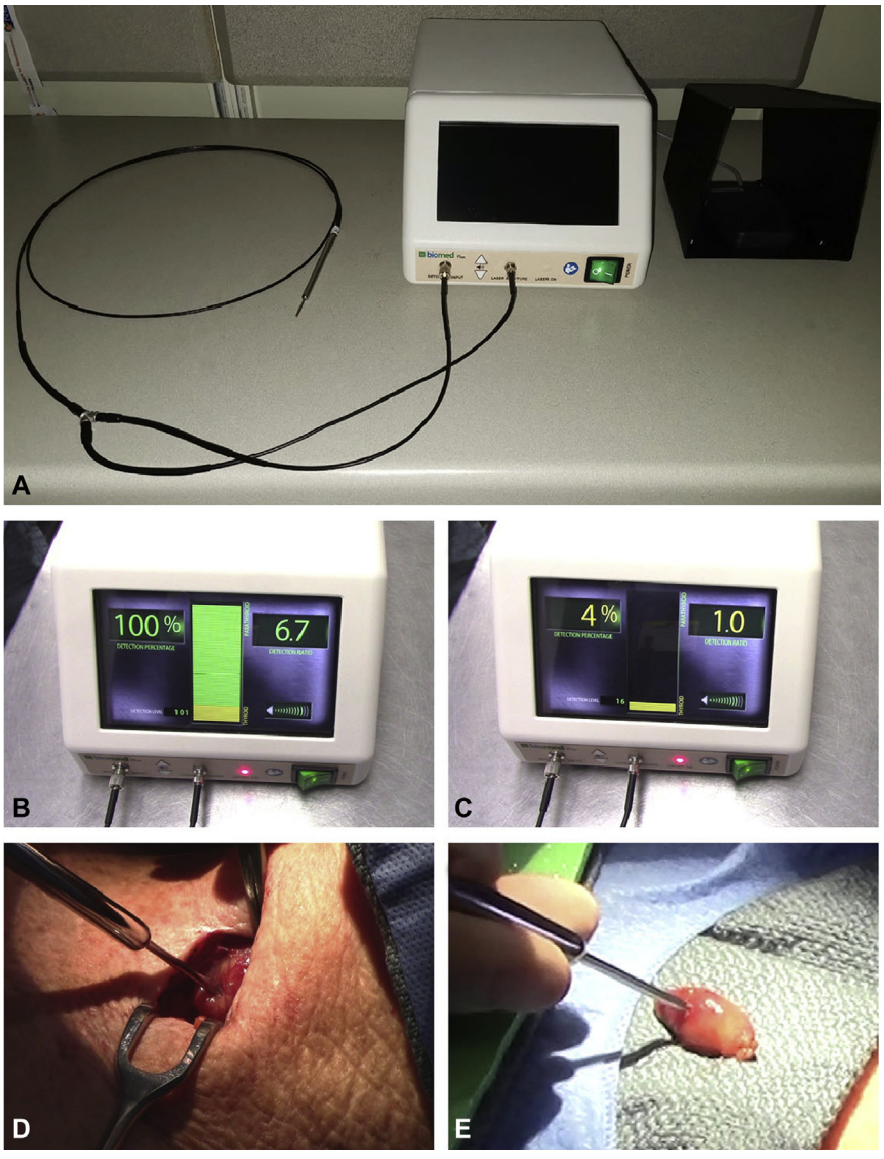

Figure 2. (A) A clinical fiber probe-based system (PTeye) used for intraoperative parathyroid gland (PG) identification, based on near infrared autofluorescence (NIRAF) detection. PTeye consists of the console that has a display and encloses the near infrared laser and the detector, a detachable fiber optic probe, and a foot-pedal that is activated by the surgeon for tissue NIRAF measurements. (B, C) The display monitor on PTeye indicates whether the tissue in contact with the probe is parathyroid (left) or not (right). (D, E) The fiber-optic probe can be used for confirming whether the tissue is parathyroid, for both in situ (left) and ex vivo (right) scenarios, with ambient operation room lights remaining on.

OR lights were switched off, ambient white-light (true color) images of the surgical field were first obtained with the camera, followed by the corresponding NIRAF (pseudo-colored green) images (Fig. 1), as described in an earlier study.[32] If the PG was removed, the same procedure was performed for excised tissues ex vivo before these specimens are sent for routine histopathology. The surgeon's expert opinion on whether an in situ or excised tissue was PG or not was first noted using only ambient white-light visualization and then recorded again after the surgeon's real-time interpretation of the acquired NIRAF images. The surgeon's confidence in identifying PG(s) before and after imaging was semi-quantitatively denoted as the 'parathyroid identification confidence

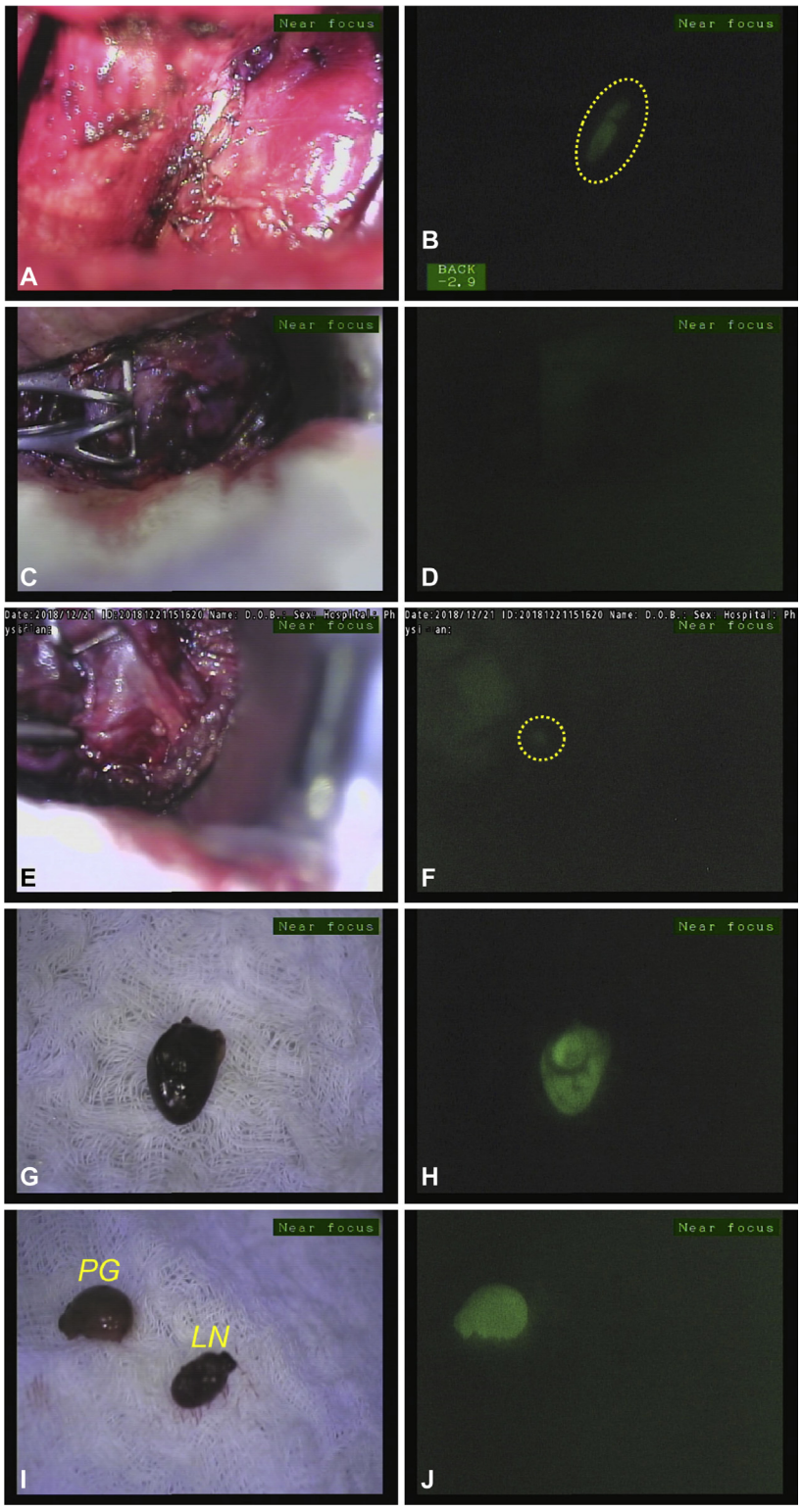

Figure 3. White-light (left) and near infrared autofluorescence (NIRAF) image in pseudo-colored green (right) taken with PDE-Neo II for (A, B) a healthy parathyroid gland (PG) in situ, (C, D) in situ thyroid lobe, (E, F) a diseased PG in situ, (G, H) a diseased PG ex vivo, and (I, J) a diseased PG and a lymph node (LN) ex vivo. Note that PG tissues exhibit stronger NIRAF compared with the nonparathyroid tissues (thyroid, lymph node) or the background.

score,' measured on a scale of 1 (very low) to 5 (very high). If tissue sites were identified with a low confidence score (2 or lower) and there was no corresponding histology available, NIRAF measurements for those sites were excluded from the study.

After image acquisition with PDE-Neo II, the surgeon repeated NIRAF assessments of the same tissue sites using PTeye with the OR lights remaining on. As the surgeon places the sterile fiber probe of PTeye on the tissue and presses the foot pedal, tissue NIRAF intensity is then displayed in real time on the device console display. During measurements with PTeye, it must be noted that the surgeon first establishes an NIRAF baseline for each patient by obtaining 5 successive NIRAF measurements on the patient's thyroid (or neck muscle, if thyroid was absent), after which subsequent measurements of detection level and detection ratio are recorded. Examples of a positive and negative measurement for PG as indicated on the PTeye display are represented in Figures 2B and 2C, respectively. All PGs evaluated in this study were surgically exposed with adequate dissection before NIRAF detection with PDE-Neo II (imaging-based) or PTeye (fiber probe-based).

Data analysis

For quantitative analysis, NIRAF images acquired with PDE-Neo II were retrospectively analyzed using Image J software (NIH) by an independent, blinded, and untrained observer. NIRAF intensity from at least 3 regions of equal dimensions within areas of maximum fluorescence (brightest region) in the image was averaged and normalized to the background noise to generate NIRAF-to-background ratio (NBR) for each image. For in situ images of potential PGs, background noise was quantified from areas of adjacent soft tissues, for example, thyroid. In contrast, when excised tissues were imaged, the background noise was measured from areas of the "nontissue background" due to lack of adjacent soft tissues in the image. Continuous variables, such as NBRs for PDE-Neo II and detection ratios (as described earlier) for PTeye, were then averaged accordingly for concurrently assessed PG tissues and non-PG tissues and reported as mean ± SE with the interquartile range (IQR). Differences in these measured ratios were analyzed using the 2-tailed *t*-test for unequal variance. A paired *t*-test was used for assessing the change in parathyroid identification confidence score from the surgeon before and after NIRAF imaging. For these analyses, a p value <0.05 was considered statistically significant. Detection rate for each system was determined by correlating the number of tissues deemed PG positive by the system (Threshold: NBR $>$ 1.10 for PDE-Neo II[32]; detection ratio >1.2 for PTeye[26,27]) with the number of PG tissues confirmed using histology for excised or biopsied PGs, or visual inspection by participant surgeons for in situ PGs (assessed with a parathyroid identification confidence score >2).

RESULTS

Patient demographics

Twenty patients assessed concurrently with both NIRAF detection-based systems were enrolled for this study, which consisted of 16 (80%) women and 4 (20%) men. Clinicopathologic features are summarized in eTable 1. Median age was 59 years (IQR 41.5 to 64.5 years), and median BMI was 27.8 kg/m^2 (IQR 24.5 to 34.1 kg/m^2). Surgical procedures included 6 total thyroidectomies (with or without central neck dissection), 3 thyroid lobectomies, 1 completion thyroidectomy, 1 completion central neck dissection (with previous total thyroidectomy), 1 combined total thyroidectomy-parathyroidectomy, and 8 parathyroidectomies. All 9 patients who underwent parathyroidectomy had preoperative ultrasound performed, and 4 patients underwent preoperative ^{99m}Tc-sestamibi nuclear imaging. Ultrasound was able to preoperatively visualize diseased PG(s) in 8 of 9 (88.9%) patients, and ^{99m}Tc-sestamibi imaging could localize hyperfunctioning PG(s) in 3 of 4 (75.0%) patients. A total of 12 PGs were excised for histologic analysis, among which 2 glands were normocellular and 10 glands were hypercellular. Among the 2 excised normocellular PGs, 1 gland was found in conjunction with thymic tissue, making it appear larger than its true size and was presumed diseased by the surgeon, and the other gland was found associated with adjacent medullary thyroid cancer in a thyroidectomy patient.

Device Performance of NIRAF-based modalities

Concurrent assessment with PDE-Neo II and PTeye was performed on 33 PGs (23 healthy and 10 diseased PGs) and 19 nonparathyroid sites (thyroid, mediastinal soft tissues, lymph nodes, and yellow and brown fat) either in situ or ex vivo for the enrolled patients. The surgical field of view as displayed on the device monitor when visualized using PDE-Neo II with ambient white light has been depicted in Figures 3A, 3C, 3E, 3G, and 3I and subsequently with corresponding NIR illumination in Figures 3B, 3D, 3F, 3H, and 3J. PG tissues were observed to have stronger NIRAF intensity than those of the nonparathyroid sites when subjectively interpreted in real time by the surgeon in the OR, as well as when the acquired NIRAF images were retrospectively and quantitatively analyzed by an independent untrained observer.

Quantitative analysis revealed that the mean NBR of PGs (n = 33) measured 1.24 ± 0.03 (IQR 1.12 to 1.31), and the mean NBR of nonparathyroid sites (n = 19) measured significantly lower at 1.12 ± 0.04 (IQR 1.00 to 1.16; p = 0.013). Mean NBR from diseased PGs measured significantly higher than that of healthy PGs (1.38 ± 0.07 vs 1.17 ± 0.02; p = 0.02). Mean NBR for PGs imaged ex vivo also measured higher than NBR quantified from in situ PGs (1.41 ± 0.08 vs 1.17 ± 0.02; p = 0.010).

Unlike PDE-Neo II, quantitative parameters, such as detection ratio, were output in real time with PTeye, as displayed in Figure 2. In agreement with results of imaging approach, the mean detection ratio with PTeye was also considerably higher for PGs at 3.55 ± 0.27 (IQR 2.06 to 4.07) compared with nonparathyroid tissues that measured 1.33 ± 0.52 (IQR 0.38 to 0.95; p = 0.0007). However, in contrast with PDE-Neo II, no significant difference was observed between detection ratios of diseased and healthy PGs at 4.06 ± 0.53 and 3.26 ± 0.29, respectively (p = 0.20). Similarly, no notable difference in detection ratios was observed between ex vivo and in situ measurements for PG specimens: 3.97 ± 0.60 vs 3.34 ± 0.27 (p = 0.35). A comparative overview of quantitative parameters, such as NBRs and detection ratio, between both the systems is provided in Table 1.

In terms of device performance for PG identification, PDE-Neo II provided 90.9% sensitivity, 73.7% specificity, and 84.6% overall accuracy (Table 2), when based on the surgeon's real-time interpretation of NIRAF images. The sensitivity of imaging in detecting NIRAF from PGs was further reflected with a significant increase in the surgeon's mean parathyroid identification confidence score. On using just ambient white light, the surgeon's confidence score stood at 3.91 ± 0.09, and improved significantly to 4.17 ± 0.02 after imaging (+0.26; p = 0.006). With retrospective quantification of the same NIRAF images analyzed post hoc by an independent observer, PDE-Neo II demonstrated 81.8% sensitivity, 73.7% specificity, and 78.8% overall accuracy in PG identification. In comparison with imaging, NIRAF detection with PTeye yielded 97.0% sensitivity, 84.2% specificity, and 92.3% overall accuracy in PG identification on the basis of real-time output of detection ratios. Of the 12 PG specimens (10 diseased and 2 healthy) that were resected and validated with histology, PG detection rate was 91.7% for PDE-Neo II (11 of 12 PGs) based on surgeon's real-time interpretation and 75.0% (9 of 12 PGs) with post-hoc analysis of NIRAF images vs 100% for PTeye (12 of 12 PGs based on device output). More importantly, real-time interpretation with PDE-Neo II as well as PTeye aided in intraoperative identification of diseased PGs that were not preoperatively localized in 11.1% of patients who had an ultrasound (1 of 9 patients) and 25.0% of patients who underwent ^{99m}Tc-sestamibi scans (1 of 4 patients).

Table 1. Overview of Near Infrared Autofluorescence-Related Quantitative Parameters Measured Concurrently with Imaging and Fiber Probe-Based Approaches

Parameter	n	Mean ± SD	p Value
NBR with PDE-Neo II (imaging-based)			
Total PG	33	1.24 ± 0.03	0.013*
Total nonparathyroid tissue	19	1.12 ± 0.04	
Healthy PG	23	1.17 ± 0.02	0.02*
Diseased PG	10	1.38 ± 0.07	
In situ PG	21	1.17 ± 0.02	0.01*
Excised PG	12	1.41 ± 0.08	
Detection ratios with PTeye (fiber probe-based)			
Total PG	33	3.55 ± 0.27	0.0007*
Total nonparathyroid tissue	19	1.33 ± 0.52	
Healthy PG	23	3.26 ± 0.29	0.20
Diseased PG	10	4.06 ± 0.53	
In situ PG	21	3.34 ± 0.27	0.35
Excised PG	12	3.97 ± 0.60	

*$p < 0.05$ (statistically significant based on 2-tailed *t*-test for unequal variance).
NBR, near infrared autofluorescence-to-background ratio; PG, parathyroid gland.

DISCUSSION

The discovery of NIRAF of PGs at Vanderbilt University has led to a surge of studies that exploited this unique property of PG tissues using modalities capable of NIRAF detection. The popularity of this method is a result of its label-free nature, thereby overcoming the limitations of intraoperative imaging typically associated with methylene blue, indocyanine green, or intraoperative scintigraphy, all of which require contrast agent injection.[33-35] As the etiology behind NIRAF in PG tissues is still being investigated,[36,37] the majority of studies have relied on detection of NIRAF for intraoperative PG identification via imaging systems, and only studies from the Vanderbilt group have used the fiber probe-based approach of NIRAF detection for the same application. The lone study that included both imaging and fiber probe-based methods of NIRAF detection did not compare the 2 approaches concurrently, and used a non-commercially available NIRAF imaging system (modified from a Karl Storz camera) in 9 patients.[27] The current study is the first to report on the direct comparison between the imaging (noncontact-based)

Table 2. Comparison of Parathyroid Gland Identification Rates and Device Performance Between PDE-Neo II (Imaging-Based) and PTeye (Fiber Probe-Based) Across 20 patients

	Imaging (PDE-Neo II camera)		
Variable	**Real-time image interpretation by expert surgeon**	**Post-hoc image analysis by independent observer**	**Fiber probe (PTeye), real-time data output**
Performance	NIRAF detection with imaging	NIRAF detection with imaging	NIRAF detection with fiber probe
PG assessed (P = 33), p/P (%)			
Identification rate	30/33 (90.9)	27/33 (81.8)	32/33 (97.0)
Healthy	20/23 (87.0)	19/23 (82.6)	22/23 (95.7)
Diseased	10/10 (100.0)	8/10 (80.0)	10/10 (100.0)
Sensitivity	30/33 (90.9)	27/33 (81.8)	32/33 (97.0)
Non-PG site assessed* (NP = 19)			
Specificity, np/NP (%)	14/19 (73.7)	14/19 (73.7)	16/19 (84.2)
Positive predictive value, %	85.7	84.4	91.4
Negative predictive value, %	82.4	70.0	94.1
False-negative rate, %	9.1	18.2	3.0
False-positive rate, %	26.3	26.3	15.8
Overall accuracy, % (kappa value)	84.6 (0.66)	78.8 (0.55)	92.3 (0.83)

*Non-PG sites assessed: thyroid lobes, lymph node, central neck or lateral neck or mediastinal tissues, and yellow and brown fat.
NIRAF, near infrared autofluorescence; np, device negative for parathyroid; NP, true negative nonparathyroid tissue; p, device positive for parathyroid; P, true positive parathyroid tissue; PG, parathyroid gland.

and fiber probe (contact-based) approaches in NIRAF detection, which was performed concurrently in a single cohort of patients for intraoperative PG identification. PDE-Neo II (Hamamatsu) and PTeye served as the representative devices for imaging and fiber probe-based systems, respectively, where both these modalities are commercially available and rely on NIRAF detection from PG tissues.

Based on our results, NIRAF of PG tissues were considerably higher than other soft tissues of the neck, including the thyroid gland, when tested with either NIRAF detection-based modalities, in agreement with earlier study observations.[16,17,19,21,26,32] On assessing the device performance in this small cohort of patients, NIRAF detection with the fiber probe-based device demonstrated a higher accuracy of 92.3% in PG identification compared with 78.8% to 84.6% yielded by the imaging-based approach (Table 2). Better sensitivity in identifying PGs with PTeye (97.0%) could be due to the fact that the fiber probe is in direct contact with the tissue, whereas the camera of the PDE-Neo II is typically held at a distance of 5 cm from the surgical field, similar to other imaging system cameras.[38] However, because the fiber probe of PTeye requires tissue contact (Figs. 2D, 2E), the modality requires the probe to be sterile before use in each patient. On the other hand, although imaging systems do not require tissue contact, the camera still requires a transparent sterile barrier drape (Fig. 1B), as contemporary NIR cameras cannot capture sensitive images beyond a distance of 45 cm (18 inches) from the surgical field, which is the recommended "sterile zone" in an OR.[39]

When comparing the performance between imaging and fiber probe-based approaches in NIRAF detection, it is also worth noting that different excitation wavelengths were used by each modality—760 nm for PDE-Neo II and 785 nm for PTeye. Although the difference in excitation wavelengths is ostensibly small, this difference can influence the intensity of NIRAF emitted by PG tissues. Illuminating the target fluorophore (in tissue) at an excitation wavelength more closely matched to its peak absorption wavelength could result in fluorescence at a greater intensity. It is currently not clear to what extent the differences in excitation wavelength between PDE-Neo II and PTeye might have impacted the performance of these 2 devices in detecting NIRAF emitted from the assessed PG tissues. However, determining the optimal excitation wavelength for PG localization/identification needs to be considered and explored further in later iterations of these devices.

A somewhat surprising finding in our study was that the accuracy of imaging in PG identification was higher when NIRAF images were interpreted in real time by an expert surgeon (more than 10 years of experience) compared with when the same images were quantitatively analyzed post hoc by an independent blinded and untrained observer. Several factors might have contributed to this unexpected finding. Primarily, the surgeon is

able to move the camera during the procedure to image an area of interest from slightly different angles, which provides a better 3-dimensional view rather than a single 2-dimensional image, as analyzed retrospectively by the independent observer. Secondly, NIRAF images as viewed by the surgeon on the monitor (for which the imaging system is optimized) might be of a better quality than the saved images that were analyzed retrospectively. Finally, NIRAF image assessment (Figs. 1C, 3F) can be subjective and misinterpreted without sufficient surgical training or experience. Therefore, PG identification with intraoperative NIRAF imaging can also partially depend on the surgeon's expertise compared with an independent untrained evaluator. While the imaging-based approach lacks real-time quantitative information or an identification threshold for confirming PGs, this limitation has been offset in the fiber probe-based modality, where PTeye provides a NIRAF-related detection level and detection ratio instantly for the end user. The comparative benefit from an imaging vs fiber probe-based approach for intraoperative PG identification needs to be validated eventually in larger cohorts and for surgeons with nominal experience.

Differences in how tissue NIRAF is normalized for PDE-Neo II (imaging) and PTeye (fiber probe) could also affect data interpretation for each system. For post-hoc quantitative analysis with imaging systems, tissue NIRAF is typically normalized to background autofluorescence to generate an NBR. This mode of normalization can have limitations, as background autofluorescence can fluctuate significantly across different anatomic sites, as well as between in situ and ex vivo locations. It should be reiterated here that in situ background autofluorescence from thyroid and other soft tissues in the neck would be higher compared with that in an ex vivo setting. Therefore, it is understandable that PGs imaged in situ yielded considerably lower NBRs than those imaged ex vivo, as observed in our study, which was also in agreement with the findings of Squires and colleagues.[32] It might also explain why NBRs quantified from diseased PGs were considerably higher than those from healthy PGs, as a majority of the diseased glands (7 of 10 PGs) were imaged ex vivo in this study, in contrast to healthy PGs that were always visualized in situ. This trend was, however, not observed with PTeye because tissue NIRAF was normalized instead to a steady parameter—the baseline thyroid NIRAF, which does not fluctuate, unlike background autofluorescence that varies across different imaging fields. Consequently, there was no significant difference observed with PTeye in the detection ratio between diseased and healthy PGs or in situ and ex vivo PGs. In addition, it should be considered that tissue NIRAF normalization to a steady baseline parameter, such as thyroid NIRAF, would be reliable only if NIRAF intensities of the 'target tissue' and 'background thyroid' were measured from the same distance by the device detectors, namely the fiber probe for PTeye or handheld camera for PDE-Neo II. Because PTeye is a contact-based approach, the distance between the fiber probe and the target tissue/thyroid is always zero, and stays constant, due to which tissue NIRAF can be reliably normalized to thyroid NIRAF, which then serves as a steady baseline parameter. In contrast, this mode of normalization might not be applicable for imaging with PDE-Neo II, as it becomes challenging for a surgeon to ensure that the device camera is held consistently at the exact same distance for tissues being imaged at all times in an OR setting. Because NIRAF intensity can fluctuate significantly between images due to variable distance between the handheld camera and tissues, it might not be accurate to normalize tissue NIRAF from a target tissue to that of the thyroid gland, either of which might have been imaged at different distances from the camera. It would be more practical to normalize tissue NIRAF to the background fluorescence measured in the same image than to thyroid NIRAF from another image when using an imaging-based approach, as with PDE-Neo II.

Both approaches of NIRAF detection—based on imaging and fiber probe—are equipped with a distinct set of salient features, as provided in Table 3. Due to lack of spatial information provided with PTeye, the surgeon needs to first visualize the "suspect PG" tissue before confirmation with the device. In comparison, imaging systems, such as PDE-Neo II and other equivalent instruments, are capable of wide-field imaging for NIRAF detection, which can be extremely valuable for spatially localizing PGs during head and neck operations. As a result, certain studies have explored the feasibility of "mapping" PGs during operative procedures with reasonable success, even being able to visualize NIRAF of PGs below layers of fibrofatty tissue by using a custom-built imaging system.[22-25] However, the ability to localize "missing" or "hidden" PGs using NIRAF detection has not been reported with consistent success across different groups. For instance, DiMarco and colleagues[37] found that the commercial imaging system used for NIRAF detection in their study failed to find the missing PGs that could not be localized by the operating surgeon. Similar findings were also observed with our current study, where PGs in patient 6 could not be visualized by the surgeon or either NIRAF detection-based modality. Disparities in the various studies, including our current findings, might be due to differences in the NIRAF detection threshold of the cameras used across these

Table 3. Overview of the Salient Features, Merits, and Demerits of Imaging vs Fiber Probe-Based Approaches in NIRAF Detection for Intraoperative Parathyroid Identification

Feature	Imaging-based approach of NIRAF detection	Fiber probe-based approach of NIRAF detection
Model	PDE-Neo II (Hamamatsu)	PTeye (AiBiomed)
Data output	NIRAF images (gray or pseudo-colored green) and white-light images (true color) on display monitor	NIRAF detection intensity, NIRAF detection ratio
Dimension	Camera unit: 8 cm × 18.2 cm × 8 cm Console: 32.2 cm × 28.3 cm × 5.5 cm (excluding display monitor and stand)	Probe: Rigid tip portion (handheld), 16 cm long Flexible portion (connected to console), 234 cm long Console: 33 cm × 21.6 cm × 14 cm
Functional component	Portable near infrared camera	Handheld fiber-optic probe for point-based NIRAF detection
Laser source	760 nm light-emitting diode	785 nm laser diode
Spatial information	Yes	None
Working distance from surgical field	5 cm (near focus) to 30 cm (far focus)	Contact-based modality
Surgical field of view per measurement	10 cm × 10 cm	600 μm-wide (point-based measurement)
Auditory feedback	No	Yes
Visual feedback	Remote display monitor	Console display interface
Contrast agents	Not required	Not required
Ambient OR light interference	Yes	No
Commercial availability	Yes	Yes
FDA approval for label-free intraoperative PG identification	Not at present for PDE-Neo II (approval granted for Fluobeam, another NIRAF imaging system)	Yes
Advantage	Wide-field imaging technique	A more compact unit
	Spatial information of parathyroid acquired	Handheld point-based guidance technique
	Multifunctional device; can be used for other surgical guidance applications in conjunction with contrast agents: lymph node surveillance, tumor margin demarcation, perfusion assessment of PG or other tissues	Provides real-time quantitative information
	—	Functional with ambient OR lights

(Continued)

Table 3. Continued

Feature	Imaging-based approach of NIRAF detection	Fiber probe-based approach of NIRAF detection
Disadvantage	Affected by ambient OR lights	No spatial information provided
	NIRAF signal affected by varying distance of camera from surgical field	Sterility of probe is required as the modality is contact-based
	No real-time quantitative information provided	Cannot localize hidden or missing PG; prospective PG needs to be visualized before assessment with device
	NIRAF image interpretation is subjective and would depend on surgeon experience	Error in baseline NIRAF acquisition could provide inaccurate results
	Wider neck incision required for NIRAF image acquisition	—
	Weaker NIRAF signal from deeper PG	—

NIRAF, near infrared autofluorescence; OR, operating room; PG, parathyroid gland.

studies. Because NIR wavelengths can typically penetrate only a few millimeters of tissue, the ability to localize missing PGs will highly depend on the camera sensitivity, the NIR irradiance used, and optical properties of the tissues that overlie the hidden PGs. Therefore, although commercially available imaging systems might be limited currently from being able to localize missing or hidden PGs, the preliminary results of Kim and colleagues[22-24] are promising, and indicate that specific iterations to imaging systems might eventually ensure NIRAF-based spatial mapping even for hidden PGs.

Because imaging with PDE-Neo II does not involve tissue contact, NIRAF detection of PG becomes problematic with increasing distance between the camera and the location of PG. As a result, localization of deep-seated PGs or ectopic PGs can require more extensive surgical dissection or wider incisions in the neck to obtain optimal NIRAF images with the camera. These issues with imaging can be further compounded when other strong sources of NIRAF—surgical kittner, surgical drape, adjacent parathyroid—are present in the surgical field of view, as they can obscure NIRAF of the main target PG. These limitations are minimized with PTeye, as the handheld fiber probe can be conveniently positioned onto the target site, irrespective of PG location or extraneous sources of NIRAF in the surgical field.

With regard to incorporating NIRAF detection approaches during surgical procedures, it must be noted that OR lights must be off before use of most imaging systems, as these tend to interfere with NIRAF detection in the surgical field, potentially disrupting conventional surgical work flow.[15,27] On the contrary, the system design of PTeye ensures that the device can measure tissue NIRAF, even in the presence of OR lights, making it a relatively easier modality to implement in a manner similar to other contact-based modalities, such as nerve-monitoring devices, already being used in head and neck operations.[40] Considering device compatibility with OR lights, a newer-generation imaging system called Fluobeam LX was showcased recently, and the device was described as being able to detect tissue NIRAF without interference from OR lights.[41] In terms of device utility for intraoperative surgical guidance, the performance of PTeye has to date been validated for label-free parathyroid identification only,[26,27] and its scope for other applications remains to be explored. On the other hand, imaging systems such as PDE-Neo II have successfully demonstrated feasibility for various applications besides parathyroid localization, such as tissue angiography, tumor margin demarcation, and lymph node mapping.[38]

Although promising results were obtained with both imaging and fiber probe-based approaches for NIRAF detection in our study, these modalities should currently serve as adjuncts for label-free intraoperative PG identification. Surgical skill and expertise should still remain pivotal for localizing, identifying, and eventually preserving PGs. At present, modalities capable of detecting NIRAF for intraoperative PG identification would probably be more beneficial for surgeons with nominal experience or training in head and neck operations,[9,10,42] patients with multigland parathyroid disease or aberrant-ectopic PGs,[11] reoperative procedures with distorted anatomy,[43] and operations for malignant thyroid disease.[44] A prime advantage gained in these scenarios would involve identifying PGs missed by preoperative localization with ultrasound or ^{99m}Tc-sestamibi scans—as demonstrated with our results—thereby minimizing frozen biopsies sent for PG confirmation, leading to potential reduction in OR procedure time and associated costs. Certain studies have investigated the impact of NIRAF detection-based imaging on patient outcomes in thyroid and parathyroid operations by using different commercial systems, such as Fluobeam and PDE-Neo II with variable results,[20,29,32,37] while outcomes studies using fiber probe-based approaches (ie PTeye) are currently underway. However, there is an additional need to conduct larger, long-term outcomes studies that would evaluate the cost-to-benefit ratio associated with the use of modalities that can detect NIRAF to minimize postsurgical morbidity and unnecessary expenses.

CONCLUSIONS

Two different optical modalities based on NIRAF detection were found to potentially serve as valuable tools for sensitively identifying healthy and diseased PGs intraoperatively, and could be of substantial benefit in ensuring optimal patient outcomes after thyroid and parathyroid operations. Imaging based on NIRAF detection can guide PGs localization in relation to adjacent anatomic structures by providing valuable spatial information. In parallel, fiber probe-based NIRAF detection can successfully provide real-time quantitative information that can aid in objectively confirming PG tissue in real time, even in the presence of ambient OR lights.

Author Contributions

Study conception and design: Thomas, Squires, Metcalf, Mahadevan-Jansen, Phay
Acquisition of data: Squires, Metcalf, Phay
Analysis and interpretation of data: Thomas, Squires, Metcalf, Mahadevan-Jansen, Phay
Drafting of manuscript: Thomas
Critical revision: Thomas, Squires, Metcalf, Mahadevan-Jansen, Phay

Acknowledgment: The authors would like to thank the OR staff for their assistance in data collection.

REFERENCES

1. Antakia R, Edafe O, Uttley L, Balasubramanian SP. Effectiveness of preventative and other surgical measures on hypocalcemia following bilateral thyroid surgery: a systematic review and meta-analysis. Thyroid 2014;25:95–106.
2. Edafe O, Antakia R, Laskar N, et al. Systematic review and meta-analysis of predictors of post-thyroidectomy hypocalcaemia. Br J Surg 2014;101:307–320.
3. Simental A, Ferris RL. Reoperative parathyroidectomy. Otolaryngol Clin North Am 2008;41:1269–1274.
4. Cron DC, Kapeles SR, Andraska EA, et al. Predictors of operative failure in parathyroidectomy for primary hyperparathyroidism. Am J Surg 2017;214:509–514.
5. Doherty GM, Weber B, Norton JA. Cost of unsuccessful surgery for primary hyperparathyroidism. Surgery 1994;116:954–958.
6. Wachtel H, Cerullo I, Bartlett EK, et al. What can we learn from intraoperative parathyroid hormone levels that do not drop appropriately? Ann Surg Oncol 2015;22:1781–1788.
7. Mohebati A, Shaha AR. Imaging techniques in parathyroid surgery for primary hyperparathyroidism. Am J Otolaryngol 2012;33:457–468.
8. Ahuja AT, Wong KT, Ching ASC, et al. Imaging for primary hyperparathyroidism—what beginners should know. Clin Radiol 2004;59:967–976.
9. Sosa JA, Bowman HM, Tielsch JM, et al. The importance of surgeon experience for clinical and economic outcomes from thyroidectomy. Ann Surg 1998;228:320–330.
10. Sosa JA, Powe NR, Levine MA, et al. Thresholds for surgery and surgical outcomes for patients with primary hyperparathyroidism: a national survey of endocrine surgeons. J Clin Endocrinol Metab 1998;83:2658–2665.
11. Chen H, Wang TS, Yen TWF, et al. Operative failures after parathyroidectomy for hyperparathyroidism: the influence of surgical volume. Ann Surg 2010;252:691–695.
12. Novis DA, Zarbo RJ. Interinstitutional comparison of frozen section turnaround time. Arch Pathol Lab Med 1997;121:559.
13. Paras C, Keller M, White L, et al. Near-infrared autofluorescence for the detection of parathyroid glands. J Biomed Optics 2011;16:067012.
14. McWade MA, Paras C, White LM, et al. A novel optical approach to intraoperative detection of parathyroid glands. Surgery 2013;154:1371–1377.
15. McWade MA, Paras C, White LM, et al. Label-free intraoperative parathyroid localization with near-infrared autofluorescence imaging. J Clin Endocrinol Metab 2014;99:4574–4580.
16. McWade MA, Sanders ME, Broome JT, et al. Establishing the clinical utility of autofluorescence spectroscopy for parathyroid detection. Surgery 2016;159:193–203.
17. Ladurner R, Sommerey S, Arabi NA, et al. Intraoperative near-infrared autofluorescence imaging of parathyroid glands. Surg Endosc 2017;31:3140–3145.

18. Ladurner R, Al Arabi N, Guendogar U, et al. Near-infrared autofluorescence imaging to detect parathyroid glands in thyroid surgery. Ann R Coll Surg Engl 2018;100:33–36.
19. Falco J, Dip F, Quadri P, et al. Increased identification of parathyroid glands using near infrared light during thyroid and parathyroid surgery. Surg Endosc 2017;31:3737–3742.
20. Dip F, Falco J, Verna S, et al. Randomized controlled trial comparing white light with near-infrared autofluorescence for parathyroid gland identification during total thyroidectomy. J Am Coll Surg 2019;228:744–751.
21. Shinden Y, Nakajo A, Arima H, et al. Intraoperative identification of the parathyroid gland with a fluorescence detection system. World J Surg 2017;41:1506–1512.
22. Kim SW, Song SH, Lee HS, et al. Intraoperative real-time localization of normal parathyroid glands with autofluorescence imaging. J Clin Endocrinol Metab 2016;101:4646–4652.
23. Kim SW, Lee HS, Ahn Y-C, et al. Near-infrared autofluorescence image-guided parathyroid gland mapping in thyroidectomy. J Am Coll Surg 2018;226:165–172.
24. Kim SW, Lee HS, Lee KD. Intraoperative real-time localization of parathyroid gland with near infrared fluorescence imaging. Gland Surg 2017;6:516.
25. Kim Y, Kim SW, Lee KD, Ahn Y-C. Real-time localization of the parathyroid gland in surgical field using Raspberry Pi during thyroidectomy: a preliminary report. Biomed Optics Express 2018;9:3391–3398.
26. Thomas G, McWade MA, Paras C, et al. Developing a clinical prototype to guide surgeons for intraoperative label-free identification of parathyroid glands in real time. Thyroid 2018;28:1517–1531.
27. Thomas G, McWade MA, Nguyen JQ, et al. Innovative surgical guidance for label-free real-time parathyroid identification. Surgery 2019;165:114–123.
28. Kahramangil B, Dip F, Benmiloud F, et al. Detection of parathyroid autofluorescence using near-infrared imaging: a multicenter analysis of concordance between different surgeons. Ann Surg Oncol 2018;25:957–962.
29. Benmiloud F, Rebaudet S, Varoquaux A, et al. Impact of autofluorescence-based identification of parathyroids during total thyroidectomy on postoperative hypocalcemia: a before and after controlled study. Surgery 2018;163:23–30.
30. US FDA. FDA permits marketing of two devices that detect parathyroid tissue in real-time during surgery. Available at: https://www.fda.gov/NewsEvents/Newsroom/PressAnnouncements/ucm624982.htm. Accessed November 3, 2018.
31. Voelker R. Devices help surgeons see parathyroid tissue. JAMA 2018;320:2193.
32. Squires MH, Jarvis R, Shirley LA, Phay JE. Intraoperative parathyroid autofluorescence detection in patients with primary hyperparathyroidism. Ann Surg Oncol 2019;26:1142–1148.
33. Han N, Bumpous JM, Goldstein RE, et al. Intra-operative parathyroid identification using methylene blue in parathyroid surgery. Am Surg 2007;73:820–823.
34. Zaidi N, Bucak E, Yazici P, et al. The feasibility of indocyanine green fluorescence imaging for identifying and assessing the perfusion of parathyroid glands during total thyroidectomy. J Surg Oncol 2016;113:775–778.
35. Koc ZP, Ozcan Kara P, Dag A, Berkesoglu M. Feasibility of portable gamma camera imaging in intraoperative radioguided parathyroid adenoma identification. Iran J Nucl Med 2018;26:62–65.
36. Thomas G, McWade MA, Sanders ME, et al. Identifying the novel endogenous near-infrared fluorophore within parathyroid and other endocrine tissues. In: Opt Tomogr Spectr. Washington, DC: Optical Society of America; 2016:PTu3A.
37. DiMarco A, Chotalia R, Bloxham R, et al. Autofluorescence in parathyroidectomy: signal intensity correlates with serum calcium and parathyroid hormone but routine clinical use is not justified. World J Surg 2019;43:1532–1537.
38. Zhu B, Sevick-Muraca E. A review of performance of near-infrared fluorescence imaging devices used in clinical studies. Br J Radiol 2014;88[1045]:20140547.
39. Price P, Frey KB. Microbiology for Surgical Technologists. Boston, MA: Cengage Learning; 2003.
40. Angelos P. Recurrent laryngeal nerve monitoring: state of the art, ethical and legal issues. Surg Clin 2009;89:1157–1169.
41. Fluobeam LX: A breakthrough innovation for thyroid and parathyroid surgery. Available at: https://fluoptics.com/en/fluobeam-lx-breakthrough-innovation-thyroid-surgery/. Accessed March 29, 2019.
42. Adam MA, Thomas S, Youngwirth L, et al. Is there a minimum number of thyroidectomies a surgeon should perform to optimize patient outcomes? Ann Surg 2017;265:402–407.
43. Lin DT, Patel SG, Shaha AR, et al. Incidence of inadvertent parathyroid removal during thyroidectomy. Laryngoscope 2002;112:608–611.
44. Bergamaschi R, Becouarn G, Ronceray J, Arnaud JP. Morbidity of thyroid surgery. Am J Surg 1998;176:71–75.

APPENDIX

eTable 1. Demographics and Study Data of Each Patient in the Study Cohort (n = 20) Evaluated Concurrently with PDE Neo II and PTeye for Intraoperative Parathyroid Gland Identification

Patient no.	Disease	Age, y	Sex	BMI, kg/m^2	Preoperative USG	Preoperative ^{99m}Tc-sestamibi	Procedure	Healthy/diseased PG according to expert surgeon	PG histology	I or E	PG identification with NIRAF detection, Y/N			Expert surgeon confidence, scale: 1 to 5 (very low to very high)	
											PDE Neo II		PTeye		
											In real time?	Post-hoc analysis?	In real time?	Before NIRAF imaging (visual examination)	After NIRAF imaging
1	Graves' disease	59	M	27.3	NA	NA	TT	Healthy	Not available	I	Y	Y	Y	2	4
2	Primary hyperparathyroidism	42	F	28.3	+	+	PT	Diseased	Hypercellular	E	Y	Y	Y	4	4.5
3	Papillary thyroid cancer	41	F	22.7	NA	NA	Completion TL	Healthy	Not available	I	Y	Y	Y	4.5	4.5
4	Benign multinodular goiter	59	F	35.1	NA	NA	Rt TL	Healthy	Not available	I	Y	Y	Y	3	4
5	Primary hyper-parathyroidism	52	F	23.5	NA	NA	PT	Healthy	Not available	I	Y	Y	Y	4	4.5
					NA	NA		Diseased	Normocellular	E	Y	Y	Y	4	4
					+	NA		Diseased	Hypercellular	E	Y	Y	Y	4	4.5
6	Papillary thyroid cancer	30	M	41.7	NA	NA	Repeat CND and Rt MRND	None seen	Not available	—	—	—	—	—	—
7	Primary hyperparathyroidism	64	F	26.0	+	+	PT	Diseased	Hypercellular	E	Y	Y	Y	3.5	3.5
					NA	NA		Healthy	Not available	I	Y	Y	Y	3.5	4
8	Papillary thyroid cancer	23	F	21.6	NA	NA	Rt TL	Healthy	Not available	I	Y	Y	Y	4.5	4.5
					NA	NA		Healthy	Not available	I	Y	Y	Y	4	4.5
9	Medullary thyroid cancer	22	F	18.8	NA	NA	TT	Healthy	Not available	I	N	N	Y	4	3
					NA	NA		Healthy	Not available	I	N	N	Y	3	2
					Same PG	Same PG			Normocellular	E	N	N	Y	—	—

(Continued)

eTable 1. Continued

Patient no.	Disease	Age, y	Sex	BMI, kg/m^2	Preoperative USG	Preoperative ^{99m}Tc-sestamibi	Procedure	Healthy/diseased PG according to expert surgeon	PG histology	I or E	PG identification with NIRAF detection, Y/N			Expert surgeon confidence, scale: 1 to 5 (very low to very high)	
											PDE Neo II		PTeye		
								Same PG ex vivo			In real time?	Post-hoc analysis?	In real time?	Before NIRAF imaging (visual examination)	After NIRAF imaging
10	MEN2A with Hashimoto's thyroiditis	65	F	41.7	NA	NA	TT	Healthy	Not available	I	Y	Y	Y	4.5	5
					NA	NA		Healthy	Not available	I	Y	Y	Y	4.5	5
					NA	NA		Healthy	Not available	I	Y	Y	Y	3	3
11	Primary hyperparathyroidism	59	F	28.9	+	NA	PT	Diseased	Hypercellular	E	Y	Y	Y	4	4.5
12	Primary hyperparathyroidism	81	M	21.5	+	NA	PT	Diseased	Hypercellular	E	Y	Y	Y	4	4.5
13	Benign multinodular goiter	61	F	33.1	NA	NA	TT	Healthy	Not available	I	Y	Y	Y	4	4.5
					NA	NA		Healthy	Not available	I	Y	Y	Y	4	4.5
14	Papillary thyroid cancer with Hashimoto's thyroiditis	23	M	25.6	NA	NA	TT with CND and Rt MRND	Healthy	Not available	I	Y	N	Y	4	4.5
					NA	NA		Healthy	Not available	I	Y	N	Y	4	4.5
					NA	NA		Healthy	Not available	I	N	Y	N	4	3
15	Primary hyperparathyroidism	68	F	39.0	+	NA	PT	Diseased	Hypercellular	E	Y	Y	Y	4	4.5
16	Primary hyperparathyroidism	58	F	26.4	NA	NA	PT	Healthy	Not available	I	Y	Y	Y	4	4.5

(Continued)

eTable 1. Continued

Patient no.	Disease	Age, y	Sex	BMI, kg/m^2	Preoperative USG	Preoperative ^{99m}Tc-sestamibi	Procedure	Healthy/ diseased PG according to expert surgeon	PG histology	I or E	PG identification with NIRAF detection, Y/N			Expert surgeon confidence, scale: 1 to 5 (very low to very high)	
											PDE Neo II		PTeye		
											In real time?	Post-hoc analysis?	In real time?	Before NIRAF imaging (visual examination)	After NIRAF imaging
					+	+		Diseased		I	Y	N	Y	4	4.5
					Same PG	Same PG		Same PG ex vivo	Hypercellular	E	Y	Y	Y	—	—
17	Multinodular goiter with Hashimoto's thyroiditis and primary hyperparathyroidism	56	F	42.4	−	NA	TT with PT	Diseased		I	Y	Y	Y	4	4.5
					Same PG	Same PG		Same PG ex vivo	Hypercellular	E	Y	Y	Y	—	—
					−	NA		Diseased		I	Y	Y	Y	4	4.5
					Same PG	Same PG		Same PG ex vivo	Hypercellular	E	Y	Y	Y	—	—
18	Primary hyperparathyroidism	82	F	32.2	+	−	PT	Diseased	Hypercellular	E	Y	N	Y	4	4.5
19	Medullary thyroid cancer with Hashimoto's thyroiditis	67	F	27.0	NA	NA	TT	Healthy	Not available	I	Y	Y	Y	4.5	4.5
					NA	NA		Healthy	Not available	I	Y	Y	Y	4.5	4.5
					NA	NA		Healthy	Not available	I	Y	Y	Y	4.5	4.5
20	Benign multinodular goiter	61	F	29.9	NA	NA	Rt TL	Healthy	Not available	I	Y	Y	Y	4.5	4.5

CND, central neck dissection; E, ex vivo; F, female; I, in situ; Lt, left; M, male; ^{99m}Tc, technetium 99m; MEN2A, multiple endocrine neoplasia 2A; MRND, modified radical neck dissection; N, no; NA, not applicable; NIRAF, near infrared autofluorescence; PG, parathyroid gland; PT, parathyroidectomy; Rt, right; TL, thyroid lobectomy; TT, total thyroidectomy; USG, ultrasonography; Y, yes.